HHS Public Access

Author manuscript

Cell Stem Cell. Author manuscript; available in PMC 2023 March 03.

Published in final edited form as:

Cell Stem Cell. 2022 March 03; 29(3): 460–471.e3. doi:10.1016/j.stem.2022.01.002.

Cone photoreceptors in human stem cell derived retinal organoids demonstrate intrinsic light responses that mimic those of primate fovea

Aindrila Saha[1,2,3], **Elizabeth Capowski**[4], **Maria A. Fernandez Zepeda**[4], **Emma C. Nelson**[4], **David M. Gamm**[2,3,4,5], **Raunak Sinha**[1,2,3,5]

[1]Department of Neuroscience, University of Wisconsin, Madison, USA

[2]McPherson Eye Research Institute, University of Wisconsin, Madison, USA

[3]Cellular and Molecular Biology Training Program, University of Wisconsin, Madison, USA

[4]Waisman Center, University of Wisconsin, Madison, USA

[5]Department of Ophthalmology and Visual Sciences, University of Wisconsin, Madison, USA

SUMMARY

High-definition vision in humans and nonhuman primates is initiated by cone photoreceptors located within a specialized region of the retina called the fovea. Foveal cone death is the ultimate cause of central blindness in numerous retinal dystrophies, including macular degenerative diseases. 3D retinal organoids (ROs) derived from human pluripotent stem cells (hPSCs) hold tremendous promise to model and treat such diseases. To achieve this goal, RO cones should elicit robust and intrinsic light-evoked electrical responses (i.e., phototransduction) akin to adult foveal cones, which has not yet been demonstrated. Here, we show strong, graded, repetitive, and wavelength-specific light-evoked responses from RO cones. The photoresponses and membrane physiology of a significant fraction of these lab-generated cones are comparable with those of intact ex-vivo primate fovea. These results greatly increase confidence in ROs as potential sources of functional human cones for cell replacement therapies, drug testing and in vitro models of retinal dystrophies.

eTOC Blurb

Correspondence should be addressed to Raunak Sinha (raunak.sinha@wisc.edu).

AUTHOR CONTRIBUTIONS

The experiments were conceived and designed by R.S., D.G and E.C. All electrophysiology experiments were conducted by A.S, and R.S. Organoid generation, immunohistochemistry and electron microscopy was performed by M.Z., E.N. and E.C. Data were analyzed by A.S. and E.C. A.S., E.C., D.G. and R.S contributed to writing the manuscript.

Lead contact: Raunak Sinha

DECLARATION OF INTERESTS

David Gamm is an inventor on patents related to generation of 3D retinal organoids (US PTO no. 9,328,328) filed by the Wisconsin Alumni Research Foundation, Madison, WI. David Gamm has an ownership interest in and receives grant funding from Opsis Therapeutics, LLC, which has licensed the technology to generate 3D retinal organoids. The terms of this arrangement have been reviewed and approved by the University of Wisconsin-Madison in accordance with its conflict-of-interest policies.

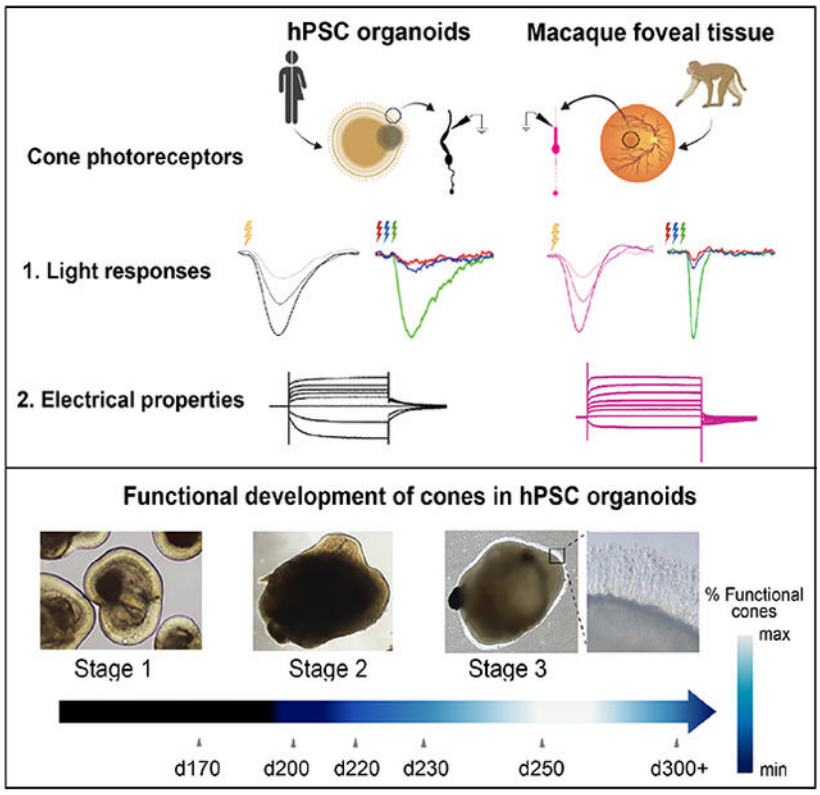

Sinha and colleagues show that human stem cell derived retinal organoids contain cone photoreceptors that possess intrinsic light sensitivity with complex electrophysiological attributes that approach those of adult primate foveal cones.

Keywords

Retinal organoid; pluripotent stem cell; fovea; cone photoreceptors; phototransduction; primate retina

INTRODUCTION

High-acuity vision in humans originates in a specialized region of the central retina called the fovea – a small anatomical feature comprised entirely of cone photoreceptors (in the central 1–2 degrees of visual field) and unique to diurnal primates among mammals (Bringmann et al., 2018; Hughes, 1977; Provis et al., 2013). Cone photoreceptors mediate daylight and color vision and are located throughout the retina, but those within the fovea are specialized and densely packed to form an exquisite ‘high definition’ pixel array (Curcio et al., 1990; Zhang et al., 2015). In contrast, rod photoreceptors mediate dim light vision and are excluded from the center of the fovea (Curcio et al., 1990; Zhang et al., 2015). Regardless of location or species, cones and rods represent specialized unipolar neurons that possess inner and outer segments, the latter containing stacks of flattened membrane organelles called discs that harbors all the biochemical machinery underlying phototransduction (Ingram et al., 2016; Palczewski, 2012).

Many conditions leading to retinal degeneration, including those that ultimately affect the fovea (e.g., macular degenerative diseases), involve dysfunction and eventual death of the cones, leading to blindness. No treatment options exist for most patients with such conditions. However, the advent of human pluripotent stem cell (hPSC) technology, along with recent advances in retinal differentiation protocols, has made it possible to envision cone cell replacement as a therapeutic option for patients with a wide range of retinal dystrophies (Ludwig and Gamm, 2021). In particular, hPSCs have been successfully differentiated into 3D retinal organoids (ROs) that have a multi-layered laminar structure with a ratio of rod and cone photoreceptors in the outer layer similar to that of the human para- or perifovea (Capowski et al., 2019; O'Hara-Wright and Gonzalez-Cordero, 2020). ROs not only hold promise as a renewable source for photoreceptor cell replacement, but also for modeling human degenerative diseases that target photoreceptors, and for screening and testing drugs and gene therapies (Bell et al., 2020; Capowski et al., 2019; Cowan et al., 2020; Gamm et al., 2013; Kruczek and Swaroop, 2020).

During differentiation, ROs can be categorized into three distinct developmental stages based on light microscopic appearance: stage 1, during which neural retinal progenitor cells (NPRCs) undergo proliferation and differentiation into early retinal cell types including photoreceptor progenitors and cones; stage 2, a period of NRPC differentiation into all remaining retinal cell types, including photoreceptors; and stage 3, which is delineated by the appearance of hair-like photoreceptor outer segments on the surface of ROs (Figure. S1A; (Capowski et al., 2019). Several reports have shown that stage 3 ROs contain highly differentiated cones that express several components of the phototransduction cascade (Capowski et al., 2019; Cowan et al., 2020; Kim et al., 2019; Meyer et al., 2011; Zhong et al., 2014). At an ultrastructural level, studies have also shown the presence of disks in RO photoreceptor outer segments, which are attached to mitochondria-rich inner segments via connecting cilia (Capowski et al., 2019; Cowan et al., 2020; Kim et al., 2019; Parfitt et al., 2016; Wahlin et al., 2017). Stage 3 ROs also contain distinct second-order neuron types – bipolar cells and horizontal cells - and ultrastructural evidence further demonstrates that photoreceptor axon terminals in mature ROs have specialized ribbon synapses (Capowski et al., 2019; Cowan et al., 2020; Wahlin et al., 2017) characteristic of vertebrate photoreceptors (Hoon et al., 2014). However, to date, evidence of light-evoked photoreceptor or neuronal function in ROs is sparse and orders of magnitude weaker than light responses in the adult primate retina (Angueyra and Rieke, 2013; Baudin et al., 2019; Cowan et al., 2020; Hallam et al., 2018; Zhong et al., 2014). Furthermore, there has been no direct demonstration of intrinsic light-evoked photoreceptor function in ROs, which is necessary to support future use of ROs as in vitro models of human retinal diseases and as sources of authentic human cones for transplantation. Lastly, prior studies of light-evoked photoreceptor function in ROs (Cowan et al., 2020; Zhong et al., 2014) lacked a systematic comparison with the gold standard for analyzing foveal cone function – intact primate fovea explants. Herein, we demonstrate graded, repetitive, wavelength-specific, light-evoked electrical responses in a significant fraction of cone photoreceptors across multiple ROs from different cell lines, which show comparable response properties and membrane physiology to that of cones in *ex vivo* primate fovea from macaque retina.

RESULTS

Cones in stage 3 hPSC-derived retinal organoids exhibit light-evoked phototransduction with similarities to cones in the adult primate retina

To assess if hPSC-derived cone photoreceptors are capable of generating physiological electrical responses to light stimuli, we generated ROs from four hPSC lines (Table S1) according to a previously published protocol (Capowski et al., 2019). We then matured the ROs to stage 3 and further maintained them in culture for a total of 240–270 days (see Methods; Figure S1A–B), a point at which they uniformly exhibit an advanced state of photoreceptor morphology and organization, including formation of inner and outer segments with expression and proper localization of key phototransduction proteins (Figure 1A; Figure S1B). Rods and cones can be easily distinguished in stage 3 ROs based on their distinct morphology, which mimics that found in primate retina (Figure S1C). The outer segments of RO cone photoreceptors (Figure 1B–C; Figure S1A) correctly localized key proteins involved in the cone phototransduction cascade, such as medium and long wavelength-sensitive photopigments (M/L opsin, Figure 1Ai), cyclic nucleotide gated ion channels (CNGB3, Figure 1Aii), and cone arrestin 3 (ARR3, Figure 1Aiii), consistent with previous studies (Capowski et al., 2019; Cowan et al., 2020; Wahlin et al., 2017; Zhong et al., 2014). For patch-clamp electrophysiological recordings, we specifically targeted cones, as determined by the distinct appearance of their inner segments which were significantly larger than those of rods (Figure S1C). The ratio of rods to cones in these ROs is approximately 4:1 (Figure S1D; Table S1), (Capowski et al., 2019; Kallman et al., 2020), similar to that found in the primate parafovea (Curcio et al., 1990; Wells-Gray et al., 2016), a region targeted in the pathogenesis of age-related macular degeneration (Schmitz-Valckenberg et al., 2016; Wilde et al., 2017). We next performed transmission electron microscopy (TEM) to look at the ultrastructural morphology of RO photoreceptors (Figure. S1E). The electron micrographs show evidence of partially stacked discs in photoreceptor outer segments, proper inner segment morphology as well as presence of ribbon synapses at photoreceptor axon terminals in the ROs (Figure. S1E–G), similar to previous reports (Capowski et al., 2019; Cowan et al., 2020; Wahlin et al., 2017). Based on these findings, we sought to compare cone sensitivities in mature ROs to those in the intact adult macaque fovea.

All electrophysiology experiments in ROs were performed without the addition of external chromophore (9-cis retinal), unlike previous studies (Cowan et al., 2020; Zhong et al., 2014). Thus, the light responses we observed in cones were generated by endogenous chromophore synthesized in ROs during differentiation using vitamin A continuously provided by B27 supplement in the culture medium (Brewer et al., 1993). At the start of each cone recording, we sequentially presented bright light flashes using LEDs with distinct peak wavelengths such that they preferentially excite one of the three cone opsin photopigments (see Methods). This cone typing light flash allowed us to identify the cone spectral type, with most recorded cones displaying a medium wavelength sensitivity (i.e., green cones) (Figure 1B) and a few cones possessing short (blue cones) or long-wavelength (red cones) sensitivity (Figure S2). We recorded from over 100 cones across multiple stage 3 ROs differentiated from four hPSC lines (Table S1), and ~35% of the cones exhibited robust

light-evoked voltage responses (Figure 1D). We also recorded from rod photoreceptors in stage 3 ROs but there were no measurable intrinsic light-evoked responses (Figure S3A). Unlike cones in ROs, rods exhibited very small voltage-dependent ionic currents (Figure. S3B). This may explain the general lack of evidence for rod function in ROs, although one study reported weak light sensitivity from a small percentage of RO rods in the presence of external chromophore (Zhong et al., 2014). The voltage responses to the typing light flashes in the RO cones replicated key features of a typical light-evoked response measured from cones in macaque fovea (within 1 mm from the foveal pit; Figure 1C), and more generally to light responses measured from cones in other vertebrate species (Baudin et al., 2019; Burkhardt, 1994; Howlett et al., 2017; Ingram et al., 2019; Matthews et al., 1990; Rieke and Baylor, 2000; Schneeweis and Schnapf, 1995). We observed light-induced hyperpolarization of the cone membrane voltage followed by repolarization to the baseline resting membrane potential, indicating that the phototransduction cascade was activated upon light onset and inactivated after cessation of the light stimulus (Figure 1B). This finding further shows that RO cones possess the necessary G-protein-mediated signaling cascade downstream of receptor activation necessary to ultimately lead to closure of cGMP-gated (CNG) ion channels, followed by inactivation of the cascade and recovery of the CNG channels from a closed to an open state upon light offset. We next measured light responses from cones in ROs across varying intensities of light flashes (Figure 1G–H). The amplitude of the light responses for individual cones (two are shown in Figure 1Gi and 1Gii) increased proportionately with the intensity of the light flash, and the amplitude vs. intensity plot was well-described by a log-linear relationship (Figure 1H) typical of vertebrate cones (Ingram et al., 2019). The temporal shape of the RO cone light responses mimicked that of vertebrate cones, albeit with a slower time course. To determine how comparable the light responses of cones in ROs are to those of cones in adult primate retina, we performed patch-clamp recordings of light-evoked responses from cones in intact macaque fovea as previously described (Figure 1C) (Baudin et al., 2019; Sinha et al., 2017). Surprisingly, the light responses of some RO cones were comparable in amplitude and kinetics to that of cones in macaque fovea (Figure 1E, F), although on average the amplitude and kinetics of the RO cone light responses was smaller and slower, respectively, than those of macaque foveal cones (Figure 1E, F). Overall, our results reveal the closest resemblance of light responses between RO cones and primate foveal cones (Table S2).

Light-evoked cone responses in retinal organoids at different background luminance

The aforementioned light responses from RO cones (Figure. 1) are a combination of the intrinsic light response from the individually recorded cone as well as any light-evoked signals coming from neighboring cones or rods via gap-junctional coupling, which is known to occur in primate retina (Hornstein et al., 2005; O'Brien et al., 2012). Since it is unknown if gap-junctional coupling exists between photoreceptors in ROs, we wanted to test its possible contribution towards light-evoked responses measured in cones. As rods in ROs lack any measurable light-evoked signals (Figure. S3A), they most likely don't contribute or shape the light responses recorded in RO cones. Thus, cone-cone gap junctional coupling is the only potential major source of electrical coupling between cones in ROs. To investigate this phenomenon, we performed recordings from RO cones after omitting ATP and GTP from the intracellular pipette solution. Deletion of ATP and GTP suppresses the intrinsic

phototransduction cascade, causing the cGMP-gated channels to close in the recorded cone while retaining contributions from any neighboring gap-junctionally coupled photoreceptors. This manipulation strongly suppressed light responses in the RO cones, similar to that previously observed for primate cones (Angueyra and Rieke, 2013; Sinha et al., 2017), suggesting minimal contribution of gap junctions between cone photoreceptors in ROs (Figure. S4A and B).

The light-evoked cone responses presented thus far were elicited from dark-adapted ROs. We next wanted to measure light responses from RO cones at brighter light levels when cone-mediated signaling is more prevalent. We presented a constant background light before eliciting brief flashes of light of varying intensity above the mean background light to produce a contrast increment. RO cones exhibited robust responses to these brief contrast increments that showed a marked resemblance in shape to responses recorded from *ex vivo* macaque fovea. Consistent with the above results from dark adapted RO cones, the average contrast response of RO cones in constant light was slower than similarly treated macaque foveal cones (Figure 2C–E). This difference in kinetics of the light response between RO and macaque foveal cones is reflected both in the response activation (estimated from the time taken for the response to reach peak amplitude) as well as in the inactivation of the response (estimated from the time taken for the response to reach baseline and the full width of the response at half maximal amplitude) (Figure. 2C–E). After normalizing the time to peak of the average responses in Figure. 2J the responses of RO cones and foveal cones superimposed more closely than the unnormalized responses throughout both the response onset and much of the recovery (Figure. 2K and Table S2).

Given that we observed light-evoked function from a sizeable fraction of RO cones, we next sought to probe RO cone function in further detail. Vertebrate (including macaque) cones are known to efficiently signal over a broad range of mean luminance by decreasing their gain (response amplitude per unit light intensity) proportionately with background luminance (Angueyra and Rieke, 2013; Baudin et al., 2019; Burkhardt, 1994; Cangiano et al., 2012; Matthews et al., 1990). In addition, it is known that vertebrate cones accelerate their response kinetics with increasing mean luminance (Angueyra and Rieke, 2013; Baudin et al., 2019; Cangiano et al., 2012; Dunn et al., 2007; Rieke and Baylor, 2000). This adaptation of vertebrate cone signals to mean luminance relies on well-studied negative feedback mechanisms within the phototransduction cascade that are mediated by calcium (Krizaj and Copenhagen, 2002; Nakatani and Yau, 1988). To test if RO cones were capable of luminance adaptation, we measured responses to brief light flashes across a range of background luminance (Figure 2A, B). Indeed, we observed that the response gain of RO cones decreased by ~50% between the dimmest and brightest background luminance (Figure 2F, H). The time to peak of the light responses also showed a significant decrease between the lowest and highest background luminance for RO cones (Figure 2I), which suggests that the RO cone signals became faster, similar to what is observed in macaque cones (Figure 2B) (Baudin et al., 2019). These results provide the first evidence that RO cones are capable of light adaptation, and most likely possess the calcium feedback mechanisms required for mediating light adaptation.

Presence of ion channels in retinal organoid cones and comparison of their membrane physiology with those of primate foveal cones

After demonstrating that light responses resulted in coupling of cGMP-gated ion channels to the phototransduction cascade in RO cones, we next wanted to assess the membrane physiology to determine if other cone ion channels are functional in RO cones. To do so, we measured the current-voltage relationship and passive membrane properties such as membrane capacitance, input resistance, membrane time constant, and resting membrane potential in RO cones and compared them to measurements in *ex vivo* macaque foveal cones. RO cones had large inward currents at hyperpolarized voltage steps under voltage clamp configuration, quite similar to that measured in primate foveal cones (Figure 3A–C). Previous studies attributed these large voltage dependent inward currents to hyperpolarization-activated cyclic nucleotide-gated (HCN) ion channels that are commonly present in vertebrate cones and are important for shaping the gain and kinetics of cone photovoltages (Barrow and Wu, 2009; Howlett et al., 2017). To confirm the presence of HCN channels and their functional role in RO cones, we measured the current-voltage relation in conjunction with pharmacological manipulation (Figure 3D–G). Bath application of 1 mM CsCl, a non-specific blocker of HCN channels, reduced the amplitude of the RO cone inward currents at hyperpolarized membrane potentials (Figure 3E, G). Importantly, this decrease in HCN currents due to CsCl could be reversed following wash out (Figure 3F, G). We repeated this experiment with a saturating concentration of a specific HCN channel blocker, ZD7288, which nearly abolished RO cone inward currents at hyperpolarized membrane potentials, confirming an HCN channel contribution to the currents (Figure. S4C). These results indicate robust contributions of HCN channels to RO cones consistent with previous studies in ROs (Kim et al., 2019; Li et al., 2021). To determine the role of HCN channels in shaping the photovoltages of RO cones, we measured light-evoked voltage responses before and after application of ZD7288. Interestingly, blocking HCN channels reduced the amplitude and slowed the decay time of voltage responses of RO cones without affecting the activation (Figure. S4D). This is consistent with the previously characterized role of HCN channels in regulating the light response of vertebrate cones (Barrow and Wu, 2009; Howlett et al., 2017).

To further compare the function of RO cones to macaque foveal cones, we quantified their membrane capacitance, input resistance, and the membrane time constant from the voltage ramp recordings and compared them to data derived from *ex vivo* macaque foveal cones. The membrane capacitance (Figure 3H) and input resistance (Figure 3J) were comparable to those of primate foveal cones (Table S3), but the membrane time constant was slightly higher for RO cones (Figure 3I; Table S3) and the resting membrane potential of RO cones was relatively more depolarized compared to macaque foveal cones (Figure 3K; Table S2), which could explain the differences in light response properties observed in our earlier experiments (Figures 1 and 2). Taken together, our data show that RO cones not only can demonstrate robust light-evoked function but can also mimic several features of the photo-response and membrane physiology of primate foveal cones (Table S2, 3).

Developmental timeline of cone function in retinal organoids

All of our cone physiology experiments to this point were performed using late stage 3 ROs (day 240–270 in vitro). To gain insight into the functional maturation of cones in stage 3 ROs, we measured light-evoked responses and membrane physiology of cones across six different timepoints of RO maturation from ~d170 in vitro to d310 days in vitro in a common hESC line WA09 (Figure 4). This comparison revealed several interesting features regarding functional maturation of phototransduction and biophysical properties in RO cones. First, cones begin to display intrinsic light-evoked electrical responses in early stage 3 organoids (i.e., d200–210 in vitro), soon after the appearance of photoreceptor outer segments in ROs (Figure 4A). As RO cones mature further, the fraction that exhibits measurable, intrinsic light-evoked responses also steadily increases, with the highest fraction of responders occurring between d250–260 *in vitro*, followed by a decline at our latest timepoint of d300–310 *in vitro* (Figure 4A). In addition to the fraction of light-sensitive cones, the overall sensitivity of cone light responses was highest between d250–260 *in vitro* (Figure 4B). However, the time course of the cone light responses did not differ across the various RO ages (Figure 4C). We next compared the current voltage relationship of both cone responders and non-responders at each of the different timepoints (Figure 4D). The magnitude of currents activated at hyperpolarizing membrane voltages in RO cones were larger for later time points (>d230 in vitro) than earlier time points (Figure 4E). There was no significant difference in the current-voltage relationship between RO cone responders vs non-responders at any of the time points. Next, we measured the resting membrane potential of RO cones in darkness at each of the timepoints and found small differences associated with RO maturation (Figure 4F). Noticeably, the RO cones at d230–240 in vitro were more hyperpolarized than cones at the other time points (Figure 4F). Moreover, the cone responders in d250–260 ROs were sitting at more hyperpolarized resting membrane potentials than their non-responding counterparts, with no such differences observed at any of the other time points (Figure 4F). Overall, this longitudinal comparison reveals a developmental timeline of RO cone phototransduction and identifies a time window of peak light sensitivity in RO cones.

DISCUSSION

An ideal in vitro 3D hPSC-based model of the human retina must be able to carry out light-evoked phototransduction, a defining tissue function that occurs exclusively in photoreceptor cells for image forming vision. Thus far, only two studies have provided evidence of weak light-evoked responses in a small fraction of photoreceptors in hPSC-derived ROs that were bathed with the external chromophore 9-cis-retinal to facilitate regeneration of the photopigment (Cowan et al., 2020; Zhong et al., 2014). Here, we report evidence of graded, wavelength-specific, physiological light-evoked responses from a sizeable population of cones (~35%) in mature, stage 3 ROs without external chromophore addition, as well as a systematic, direct comparison of RO cone and macaque foveal cone photoresponses and membrane physiology.

In our study, photoresponses and membrane physiology of RO cone photoreceptors replicated several fundamental features of cone function in the macaque fovea that

individually and/or collectively have not been demonstrated previously. First, light stimuli resulted in membrane hyperpolarization of RO cones, which shows that the complex, stepwise activation phase of the G-protein coupled receptor phototransduction signaling cascade is fully present and functional. This pathway begins with photopigment stimulation, which is followed by sequential activation of the G-protein (transducin), the effector enzyme (cGMP phosphodiesterase), and ultimately the cyclic-nucleotide gated channels (CNG). Second, the RO cone membrane potential repolarized to the resting membrane potential soon after the cessation of the light stimuli, which indicates that the biochemical machinery involved in the inactivation of the phototransduction cascade is also intact. In addition to the CNG channels that are coupled to the phototransduction cascade, our results provided evidence that HCN channels, which play a key role in photoreceptor signaling (Barrow and Wu, 2009; Bryman et al., 2020; Howlett et al., 2017), are present and functional in RO cones. Our results further show that the amplitude and time course of RO cone photovoltages are regulated by HCN channels, as found in *bona fide* macaque and vertebrate cones. Interestingly, the slower time course of the light responses in RO cones compared to the macaque foveal cones could potentially be caused by differences in expression of HCN channels, in addition to several other possible factors including morphological differences as mentioned below.

RO cones also possessed many dynamic electrophysiological features characteristic of primate cones. For example, RO cones demonstrated adaptation of gain, and to some extent, *in vivo*-like adaptation of kinetics in response to increase in luminance – a key feature of macaque and vertebrate cones – suggesting that the RO cone phototransduction cascade is regulated by calcium-mediated feedback mechanisms. Observed differences in light responses between lab-grown RO cones and intact primate foveal cones were surprisingly small. However, such differences could be due to the relative disorganization of outer segment disks in RO cones (Capowski et al., 2019; Cowan et al., 2020; Wahlin et al., 2017; Zhong et al., 2014), which is more typical of late fetal-stage human photoreceptors than the fully formed stacked disks of adult human photoreceptors. ROs also lack an RPE layer adjacent to the photoreceptor layer, which may also limit development of outer segments. Since the phototransduction cascade is membrane delimited, the stacked arrangement of disc membranes contributes to the high sensitivity and kinetics of photoreceptor signaling. Thus, lack of proper disc organization might explain the lower sensitivity and slower kinetics of cone light responses in ROs. The absence of adjacent RPE also points toward a major role for Müller glia as an alternative pathway for cone opsin regeneration in ROs, as has been shown previously in mammalian retina (Morshedian et al., 2019). Notably, stage 3 ROs contain a large population of Müller glia whose radially oriented processes extend outward through the photoreceptor layer to form the outer limiting membrane, which surrounds the base of rod and cone outer segments (Capowski et al., 2019). In fact, the lack of a well-defined RPE layer may explain the dearth of rod function in ROs which, unlike cones, rely solely on RPE for pigment regeneration (Wang and Kefalov, 2011). Furthermore, rods mature later than the cones (Hoon et al., 2014), so it is possible that the expression and/or function of key components of the rod phototransduction machinery, including the cyclic nucleotide channels, have not reached the threshold for light detection. Lastly, variability in RO cone outer segment size and shape could also contribute to the observed differences

in sensitivity and kinetics of light responses across RO cones. Despite these structural dissimilarities, our results provide the first comprehensive, direct evidence that the intrinsic light-driven functionality of RO cones is physiologically close to that of primate foveal cones.

In addition to replicating some of the key features of primate photoreceptor function that occur in the outer and inner segments, RO cones possess specialized ribbon synapses at their axon terminals as is typically seen in primate cones (Grunert and Martin, 2020). However, based on our single section TEM data, we were unable to definitively identify the stereotypic arrangement of a 'triad' synapse between a cone terminal and dendrites/processes of bipolar and horizontal cells. A more thorough analysis using serial electron microscopy and 3D reconstruction will be necessary to precisely determine the overall organization/arrangement of the pre- and post-synaptic partners at the organoid cone synapse and identify the extent of the stereotypic synaptic organization. Future investigations will compare the functional characteristics of synaptic signaling between cones and downstream neural circuitry in ROs with those of primate retina.

By assaying cone function across distinct stages of RO maturation, our results provide valuable insight into the time window at which phototransduction begins in cones as well as when it reaches peak sensitivity. Overall, the functional maturation of cones in ROs seems to be in line with both the morphological development and the timeline of gene expression in cones (Capowski et al., 2019; Cowan et al., 2020; Welby et al., 2017). According to recent single cell RNA sequencing studies, the developmental timeline in ROs closely matches that of human retina in vivo (Cowan et al., 2020). For instance, gene expression profiles and neuronal diversity of a 38-week RO mimics that of a newborn human retina (Cowan et al., 2020). Our evaluations of RO cone function over time suggests that the onset of cone phototransduction occurs at late fetal stages of primate retinal development with a steady increase in sensitivity into the early postnatal stages of retinal maturation. This timeline could contribute to the differences in cone function we observe between ROs and adult primate foveal retina, while the decline in RO cone sensitivity at >d300 in vitro may reflect innate limitations in the functional longevity of the RO culture system.

In summary, RO cone photoreceptors exhibited intrinsic light sensitivity at physiological light levels and mimicked several features of primate foveal cone light responses. This work not only provides support for ROs as unique and important sources of functional human cone photoreceptors for use in stem cell transplantation therapies, but also greatly extends the value of ROs as model systems to probe cone photoreceptor dysfunction in a wide range of retinal degenerative diseases including macular degeneration. Finally, our findings highlight key areas of variability in cone function and maturation that can be targeted in future studies to further improve the *in vitro* and *in vivo* utility of ROs.

Limitations of the study

A limitation of hPSC-derived ROs is the absence of a uniform RPE layer (Capowski et al., 2019) adjacent to the photoreceptor layer. There are often small patches of ectopic RPE present on ROs (Figure S1B), but they are inconsistent in size and not uniform. Lack of a well-defined RPE could contribute to the relatively disorganized cone outer segment

morphology in ROs. Thus, further efforts to improve RO technology are needed to promote proper outer segment disk formation and greater uniformity of cone maturation. Another limitation is the lack of light-evoked function in RO rods, which might be dependent on the absence of a juxtaposed RPE. Given that it is extremely difficult to obtain human foveal tissue for physiology, and human and macaque retina bear a close resemblance, we have utilized cone recordings from intact macaque fovea as a comparison for light responses with those in ROs. Finally, even though the cone to rod density of our ROs mimic that of human parafovea, RO cones lack morphological specializations found in foveal cones, such as elongated inner segments and axons (Hoang et al., 2002; Hsu et al., 1998).

STAR METHODS

RESOURCE AVAILABILITY

Lead Contact—Further information and requests for resources and reagents should be directed to the Lead Contact, Raunak Sinha (raunak.sinha@wisc.edu).

Materials availability—This study did not generate new unique reagents.

Data and code availability—The datasets supporting the current study are available from the Lead Contact on request.

EXPERIMENTAL MODEL AND SUBJECT DETAILS

Human pluripotent stem cell culture and generation of retinal organoids— Retinal organoids were generated from 4 previously characterized hPSC lines (2429, 1013, 1581 and WA09: table S1; Capowski et al. 2019). Pluripotent stem cells were maintained on Matrigel (WiCell) in mTeSR+ (Stem Cell Technologies) and passaged with ReLeSR (Stem Cell Technologies). To generate retinal organoids, embryoid bodies (EB) were lifted by incubating pluripotent stem cells with 0.7 ml ReLeSR per well at 37°C for 3–5 min on day 0 (d0). EBs were collected in mTeSR+ and incubated overnight with ROCK inhibitor Y-27632 (R&D systems) at a final concentration of 10 μM. From d2–d4, EBs were gradually weaned into Neural Induction Media (NIM: DMEM: F12 1:1, 1% N2 supplement, 1x MEM nonessential amino acids (MEM NEAA), 1x GlutaMAX and 2 μg/ml heparin (Sigma)) and on d6, BMP4 (R&D Systems) was added to a final concentration of 1.5nM. EBs were plated at a density of 200 EBs per well on Matrigel-coated 6 well plates on d7 followed by ½ media changes on d9, d12 and d15. On d16, NIM was replaced with Retinal Differentiation Media (RDM: DMEM: F12 3:1, 2% B27 supplement, MEM NEAA, 1X antibiotic, anti-mycotic and 1x GlutaMAX) and plates were fed 3X per week until d25–30 when retinal organoids formed and could be detached from the plate and collected in 3D-RDM (RDM with 5% FBS, 100 μM taurine (Sigma) and 1:1000 chemically defined lipid supplement (Thermo Fisher) added) in polyHEMA (Sigma)-coated T25 flasks (50 organoids per flask). Organoids were maintained for over 300 days with 2x per week ½ media changes with 3D-RDM. For light-evoked electrical recordings, individual organoids were transferred to a poly-HEMA coated well of a 4 well plate which was wrapped in aluminum foil and replaced in the incubator overnight to dark adapt. Overall, we have used 23 organoids in this study across different timepoints of development (Table S1).

Primate Retina—Primate tissue was obtained from Wisconsin National Primate Research Center and all use of primate tissue was in accordance with the University of Wisconsin Institutional Animal Care and Use Committee. Recordings were made from retinae from adult *Macaca fascicularis* and *Macaca mulatta* of both sexes.

METHOD DETAILS

Organoid immunocytochemistry—For immunocytochemistry, organoids were fixed in 4% paraformaldehyde (Electron Microscopy Sciences) for 40 min at room temperature, washed with PBS, cryopreserved in 30% sucrose, and sectioned on a cryostat. 15 μm sections were collected on Superfrost Plus slides (Electron Microscopy services), blocked for 1 hr at RT in 10% normal donkey serum, 5% BSA, and 0.5% Triton, then incubated overnight at 4°C with primary antibodies diluted in block. Primary antibodies, sources and dilutions are listed in key resources table. Slides were incubated with species-specific fluorophore-conjugated secondary antibodies diluted 1:500 in block, for 30 minutes in the dark at RT (donkey anti-mouse Alexa Fluor 488, donkey anti-rabbit AF546 and donkey anti goat-AF633: Thermo Fisher) and mounted with Prolong Gold antifade + DAPI to counterstain nuclei (Thermo Fisher). Sections were imaged on a Nikon A1R-HD laser scanning confocal microscope. For cone and rod counts, sections of the outer nuclear layer-like region of at least 4 individual organoids per line were immunostained with NR2E3 and cone ARR3, imaged, and rods and cones from at least 6 images were counted using Nikon Elements Analysis D software (Capowski et al., 2019; Kallman et al., 2020).

Electron microscopy—Whole organoids were fixed in 3% glutaraldehyde/1% paraformaldehyde in 0.08M sodium cacodylate buffer overnight at 4°C with gentle rocking, washed in 0.1M cacodylate and post fixed for 2 hrs at RT in 1% osmium tetroxide in 0.1M sodium cacodylate. The samples were subsequently dehydrated in a graded ethanol series followed by dehydration in propylene oxide, then embedded in Epon epoxy resin. Ultra-thin sections were cut with a Leica EM UC6 Ultramicrotome and collected on pioloform-coated 1 hole slot grids (Ted Pella Inc, cat # 19244). Sections were contrasted with Reynolds lead citrate and 8% uranyl acetate in 50% EtOH. Ultrathin sections were visualized with a Philips CM120 electron microscope and images were captured with an AMT BioSprint side mounted digital camera using AMT Capture Engine software.

Tissue Preparation and Electrophysiology—Single-cell electrical recordings were performed in the primate fovea (<1 mm from foveal center) according to previously described methods (Baudin et al., 2019; Sinha et al., 2017). For all recordings, the retina was dark adapted for at least one hour in warm oxygenated Ames medium (~32–34°C). Then, a piece of retina containing the foveal pit was isolated from the choroid and pigment epithelium and mounted flat, photoreceptor side up on a poly-lysine-coated coverslip in a recording chamber. The retina was constantly perfused with warmed and oxygenated (5% CO_2 / 95% O_2) Ames solution. After identifying the foveal pit in the retina, recordings were made from the inner segments of cones that were within 1mm of the pit. For some cone recordings, the tissue was treated with DNase (concentration, 2 mins) to make the cone inner segments more accessible. Electrical recordings from RO cones were made following the same approach as macaque foveal cones. For all recordings, the ROs were dark adapted

overnight and then transferred to warm (~32°C), oxygenated Ames solution for an hour before mounting on a poly-lysine-coated coverslip in a recording chamber. The RO was constantly perfused with warmed (~32°C) and oxygenated Ames solution. Recordings were made from cones that had an outer segment.

Photoreceptors were visualized for patch-clamp recordings using infrared light (>900 nm; Figure S1C). Voltage-clamp recordings from cones were made with glass pipettes (~10–15 MΩ) filled with an intracellular solution containing (in mM) 133 potassium aspartate, 10 KCl, 10 HEPES, 1 $MgCl_2$, 4 ATP, 0.5 GTP, pH ~7.3, ~280 mOsm (Baudin et al., 2019; Sinha et al., 2017). Data was low pass filtered at 3 kHz, digitized at 10 kHz and acquired using a Multiclamp 700B software with Symphony Data Acquisition software, an open source, MATLAB based electrophysiology software. To isolate the HCN-mediated current, 1mM CsCl (Sigma-Aldrich) diluted in oxygenated Ames solution was applied in the perfusion for 1.5–2 minutes. For recovery, cells were washed with Ames solution for at least 3–4 minutes before making measurements. The HCN-channel specific blocker, ZD7288 (Sigma-Aldrich), was applied at a concentration of 0.1 mM. Voltage-clamp recordings were performed to measure the passive membrane properties (Figure 3). Cells were presented voltage steps from −80 to −10 mV, in increasing steps of 10 mV from a holding membrane potential of −60 mV. Membrane potentials reported in this study have not been corrected for the liquid junction potential.

Light stimulation—Computer driven LEDs with peak wavelengths of 410 nm, 505 nm and 650 nm were used to deliver full-field light spot of 500 μm in diameter and focused on the photoreceptor layer through the optics of the microscope. All stimulus protocols were generated using custom written MATLAB-based extensions of Symphony Data Acquisition Software and delivered at 10 kHz. Photon densities were calibrated using estimations of primate opsin photoisomerizations (R*) per photoreceptor from measured LED spectra, cone opsin spectra (Baylor et al., 1987) and a cone collecting area of 0.37 μm^2. (Schnapf et al., 1990). At the beginning of each cone recording (Figure 1 B–F), brief light flashes from each of the three LEDs were presented sequentially to determine the cone spectral type. The recordings were made in current clamp configuration to measure membrane voltages to a range of light stimuli from complete darkness and/or with background luminance as mentioned in Figures. 1–2.

QUANTIFICATION AND STATISTICAL ANALYSIS

Cell selection criteria—For primate cone recordings, cells for data collection were chosen based on the amplitude of their typing flash responses. For current clamp recordings, cones having a typing flash response >6 mV were selected. These assumptions were based on criteria discussed and used in previous studies (Baudin et al., 2019; Sinha et al., 2017). These criteria help us streamline cells whose responses represent primate foveal cone responses in vivo. We also restricted our recording time to 5 mins post breaking into the cell to prevent washout of intracellular components, which affects quality of responses.

Analysis—All data were analyzed with custom-written MATLAB and Igor Pro analysis routines. In Figure 1H, voltage responses to flashes of different strengths of individual and average across all hPSC cones were fit with a straight line ($R^2 > 0.9$).

We used the unpaired t-test for all the statistical analysis. Error bars indicate SEM. The significance threshold was placed at $\alpha = 0.05$ (n.s., $p > 0.05$; *, $p < 0.05$; **, $p < 0.01$; ***, $p < 0.001$).

Supplementary Material

Refer to Web version on PubMed Central for supplementary material.

ACKNOWLEDGEMENTS

We thank the Wisconsin National Primate Research Center for providing macaque retinal tissue, Kim Edwards and Steven Mayerl in the Gamm lab for providing some ROs, Austin Butala and Juan Zuniga for technical support, Mrinalini Hoon and all members of the Sinha lab for their feedback on this project, and the University of Wisconsin School of Medicine and Public Health Electron Microscopy facility for assistance with the TEM. This work was supported by the NIH grants EY026070 (to R.S.), EY031411 (to R.S.), macular degeneration research award from BrightFocus foundation, young investigator grant from Alcon Research Institute, grant from E.Matilda Ziegler Foundation for the Blind, pilot grant from Wisconsin National Primate Research Center, as well as an award to R.S. (McPherson Eye Research Institute's David and Nancy Walsh Family Professorship in Vision Research); this work was also supported by NIH grant EY029890, Fight Blindness Canada 20/20, the Retina Research Foundation Emmett Humble Chair, Sarah E. Slack Prevention of Blindness Fund (a component Fund of the Muskingum County Community Foundation), the McPherson Eye Research Institute Sandra Lemke Trout Chair in Eye Research, and Research to Prevent Blindness (to D.G.). This study was supported in part by a core grant to the Waisman Center (NICHHD U54 HD090256).

11. REFERENCES

Angueyra JM, and Rieke F (2013). Origin and effect of phototransduction noise in primate cone photoreceptors. Nat Neurosci 16, 1692–1700. [PubMed: 24097042]

Barrow AJ, and Wu SM (2009). Low-conductance HCN1 ion channels augment the frequency response of rod and cone photoreceptors. J Neurosci 29, 5841–5853. [PubMed: 19420251]

Baudin J, Angueyra JM, Sinha R, and Rieke F (2019). S-cone photoreceptors in the primate retina are functionally distinct from L and M cones. Elife 8.

Baylor DA, Nunn BJ, Schnapf JL, 1987. Spectral sensitivity of cones of the monkey macaca fascicularis. The Journal of Physiology 390, 145–160. [PubMed: 3443931]

Bell CM, Zack DJ, and Berlinicke CA (2020). Human Organoids for the Study of Retinal Development and Disease. Annu Rev Vis Sci 6, 91–114. [PubMed: 32936736]

Brewer GJ, Torricelli JR, Evege EK, and Price PJ (1993). Optimized survival of hippocampal neurons in B27-supplemented Neurobasal, a new serum-free medium combination. J Neurosci Res 35, 567–576. [PubMed: 8377226]

Bringmann A, Syrbe S, Gorner K, Kacza J, Francke M, Wiedemann P, and Reichenbach A (2018). The primate fovea: Structure, function and development. Prog Retin Eye Res 66, 49–84. [PubMed: 29609042]

Bryman GS, Liu A, and Do MTH (2020). Optimized Signal Flow through Photoreceptors Supports the High-Acuity Vision of Primates. Neuron 108, 335–348 e337. [PubMed: 32846139]

Burkhardt DA (1994). Light adaptation and photopigment bleaching in cone photoreceptors in situ in the retina of the turtle. J Neurosci 14, 1091–1105. [PubMed: 8120614]

Cangiano L, Asteriti S, Cervetto L, and Gargini C (2012). The photovoltage of rods and cones in the dark-adapted mouse retina. J Physiol 590, 3841–3855. [PubMed: 22641773]

Capowski EE, Samimi K, Mayerl SJ, Phillips MJ, Pinilla I, Howden SE, Saha J, Jansen AD, Edwards KL, Jager LD, et al. (2019). Reproducibility and staging of 3D human retinal organoids across multiple pluripotent stem cell lines. Development 146.

Cowan CS, Renner M, De Gennaro M, Gross-Scherf B, Goldblum D, Hou Y, Munz M, Rodrigues TM, Krol J, Szikra T, et al. (2020). Cell Types of the Human Retina and Its Organoids at Single-Cell Resolution. Cell 182, 1623–1640 e1634. [PubMed: 32946783]

Curcio CA, Sloan KR, Kalina RE, and Hendrickson AE (1990). Human photoreceptor topography. J Comp Neurol 292, 497–523. [PubMed: 2324310]

Dunn FA, Lankheet MJ, and Rieke F (2007). Light adaptation in cone vision involves switching between receptor and post-receptor sites. Nature 449, 603–606. [PubMed: 17851533]

Gamm DM, Phillips MJ, and Singh R (2013). Modeling retinal degenerative diseases with human iPS-derived cells: current status and future implications. Expert Rev Ophthalmol 8, 213–216. [PubMed: 24039627]

Grunert U, and Martin PR (2020). Cell types and cell circuits in human and non-human primate retina. Prog Retin Eye Res, 100844. [PubMed: 32032773]

Hallam D, Hilgen G, Dorgau B, Zhu L, Yu M, Bojic S, Hewitt P, Schmitt M, Uteng M, Kustermann S, et al. (2018). Human-Induced Pluripotent Stem Cells Generate Light Responsive Retinal Organoids with Variable and Nutrient-Dependent Efficiency. Stem Cells 36, 1535–1551. [PubMed: 30004612]

Hoang QV, Linsenmeier RA, Chung CK, and Curcio CA (2002). Photoreceptor inner segments in monkey and human retina: mitochondrial density, optics, and regional variation. Vis Neurosci 19, 395–407. [PubMed: 12511073]

Hoon M, Okawa H, Della Santina L, and Wong RO (2014). Functional architecture of the retina: Development and disease. Prog Retin Eye Res 42C, 44–84.

Hornstein EP, Verweij J, Li PH, and Schnapf JL (2005). Gap-junctional coupling and absolute sensitivity of photoreceptors in macaque retina. J Neurosci 25, 11201–11209. [PubMed: 16319320]

Howlett MH, Smith RG, and Kamermans M (2017). A novel mechanism of cone photoreceptor adaptation. PLoS Biol 15, e2001210. [PubMed: 28403143]

Hsu A, Tsukamoto Y, Smith RG, and Sterling P (1998). Functional architecture of primate cone and rod axons. Vision Res 38, 2539–2549. [PubMed: 12116702]

Hughes A (1977). The topography of vision in mammals of contrasting life style: comparative optics and retinal organisation (Springer-Verlag).

Ingram NT, Sampath AP, and Fain GL (2016). Why are rods more sensitive than cones? J Physiol 594, 5415–5426. [PubMed: 27218707]

Ingram NT, Sampath AP, and Fain GL (2019). Voltage-clamp recordings of light responses from wild-type and mutant mouse cone photoreceptors. J Gen Physiol 151, 1287–1299. [PubMed: 31562185]

Kallman A, Capowski EE, Wang J, Kaushik AM, Jansen AD, Edwards KL, Chen L, Berlinicke CA, Joseph Phillips M, Pierce EA, et al. (2020). Investigating cone photoreceptor development using patient-derived NRL null retinal organoids. Commun Biol 3, 82. [PubMed: 32081919]

Kim S, Lowe A, Dharmat R, Lee S, Owen LA, Wang J, Shakoor A, Li Y, Morgan DJ, Hejazi AA, et al. (2019). Generation, transcriptome profiling, and functional validation of cone-rich human retinal organoids. Proc Natl Acad Sci U S A 116, 10824–10833. [PubMed: 31072937]

Krizaj D, and Copenhagen DR (2002). Calcium regulation in photoreceptors. Front Biosci 7, d2023–2044. [PubMed: 12161344]

Kruczek K, and Swaroop A (2020). Pluripotent stem cell-derived retinal organoids for disease modeling and development of therapies. Stem Cells 38, 1206–1215. [PubMed: 32506758]

Li L, Zhao H, Xie H, Akhtar T, Yao Y, Cai Y, Dong K, Gu Y, Bao J, Chen J, et al. (2021). Electrophysiological characterization of photoreceptor-like cells in human inducible pluripotent stem cell-derived retinal organoids during in vitro maturation. Stem Cells.

Ludwig AL, and Gamm DM (2021). Outer Retinal Cell Replacement: Putting the Pieces Together. Transl Vis Sci Technol 10, 15.

Matthews HR, Fain GL, Murphy RL, and Lamb TD (1990). Light adaptation in cone photoreceptors of the salamander: a role for cytoplasmic calcium. J Physiol 420, 447–469. [PubMed: 2109062]

Meyer JS, Howden SE, Wallace KA, Verhoeven AD, Wright LS, Capowski EE, Pinilla I, Martin JM, Tian S, Stewart R, et al. (2011). Optic vesicle-like structures derived from human pluripotent stem cells facilitate a customized approach to retinal disease treatment. Stem Cells 29, 1206–1218. [PubMed: 21678528]

Morshedian A, Kaylor JJ, Ng SY, Tsan A, Frederiksen R, Xu T, Yuan L, Sampath AP, Radu RA, Fain GL, et al. (2019). Light-Driven Regeneration of Cone Visual Pigments through a Mechanism Involving RGR Opsin in Muller Glial Cells. Neuron 102, 1172–1183 e1175. [PubMed: 31056353]

Nakatani K, and Yau KW (1988). Calcium and light adaptation in retinal rods and cones. Nature 334, 69–71. [PubMed: 3386743]

O'Brien JJ, Chen X, Macleish PR, O'Brien J, and Massey SC (2012). Photoreceptor coupling mediated by connexin36 in the primate retina. J Neurosci 32, 4675–4687. [PubMed: 22457514]

O'Hara-Wright M, and Gonzalez-Cordero A (2020). Retinal organoids: a window into human retinal development. Development 147.

Palczewski K (2012). Chemistry and biology of vision. J Biol Chem 287, 1612–1619. [PubMed: 22074921]

Parfitt DA, Lane A, Ramsden CM, Carr AF, Munro PM, Jovanovic K, Schwarz N, Kanuga N, Muthiah MN, Hull S, et al. (2016). Identification and Correction of Mechanisms Underlying Inherited Blindness in Human iPSC-Derived Optic Cups. Cell Stem Cell 18, 769–781. [PubMed: 27151457]

Provis JM, Dubis AM, Maddess T, and Carroll J (2013). Adaptation of the central retina for high acuity vision: cones, the fovea and the avascular zone. Prog Retin Eye Res 35, 63–81. [PubMed: 23500068]

Rieke F, and Baylor DA (2000). Origin and functional impact of dark noise in retinal cones. Neuron 26, 181–186. [PubMed: 10798402]

Schmitz-Valckenberg S, Sahel JA, Danis R, Fleckenstein M, Jaffe GJ, Wolf S, Pruente C, and Holz FG (2016). Natural History of Geographic Atrophy Progression Secondary to Age-Related Macular Degeneration (Geographic Atrophy Progression Study). Ophthalmology 123, 361–368. [PubMed: 26545317]

Schnapf JL, Nunn BJ, Meister M, Baylor DA, 1990. Visual transduction in cones of the monkey macaca fascicularis. The Journal of Physiology 427, 681–713. [PubMed: 2100987]

Schneeweis DM, and Schnapf JL (1995). Photovoltage of rods and cones in the macaque retina. Science 268, 1053–1056. [PubMed: 7754386]

Sinha R, Hoon M, Baudin J, Okawa H, Wong ROL, and Rieke F (2017). Cellular and Circuit Mechanisms Shaping the Perceptual Properties of the Primate Fovea. Cell 168, 413–426 e412. [PubMed: 28129540]

Wahlin KJ, Maruotti JA, Sripathi SR, Ball J, Angueyra JM, Kim C, Grebe R, Li W, Jones BW, and Zack DJ (2017). Photoreceptor Outer Segment-like Structures in Long-Term 3D Retinas from Human Pluripotent Stem Cells. Sci Rep 7, 766. [PubMed: 28396597]

Wang JS, and Kefalov VJ (2011). The cone-specific visual cycle. Prog Retin Eye Res 30, 115–128. [PubMed: 21111842]

Welby E, Lakowski J, Di Foggia V, Budinger D, Gonzalez-Cordero A, Lun ATL, Epstein M, Patel A, Cuevas E, Kruczek K, et al. (2017). Isolation and Comparative Transcriptome Analysis of Human Fetal and iPSC-Derived Cone Photoreceptor Cells. Stem Cell Reports 9, 1898–1915. [PubMed: 29153988]

Wells-Gray EM, Choi SS, Bries A, and Doble N (2016). Variation in rod and cone density from the fovea to the mid-periphery in healthy human retinas using adaptive optics scanning laser ophthalmoscopy. Eye (Lond) 30, 1135–1143. [PubMed: 27229708]

Wilde C, Poostchi A, Mehta RL, MacNab HK, Hillman JG, Vernon SA, and Amoaku WM (2017). Prevalence of age-related macular degeneration in an elderly UK Caucasian population-The Bridlington Eye Assessment Project: a cross-sectional study. Eye (Lond) 31, 1042–1050. [PubMed: 28282062]

Zhang T, Godara P, Blanco ER, Griffin RL, Wang X, Curcio CA, and Zhang Y (2015). Variability in Human Cone Topography Assessed by Adaptive Optics Scanning Laser Ophthalmoscopy. Am J Ophthalmol 160, 290–300 e291. [PubMed: 25935100]

Zhong X, Gutierrez C, Xue T, Hampton C, Vergara MN, Cao LH, Peters A, Park TS, Zambidis ET, Meyer JS, et al. (2014). Generation of three-dimensional retinal tissue with functional photoreceptors from human iPSCs. Nat Commun 5, 4047. [PubMed: 24915161]

HIGHLIGHTS

- Cone photoreceptors in stage 3 human ROs exhibit robust light-evoked responses
- Light responses of RO and foveal cones share similarities in sensitivity and kinetics
- Cones in ROs exhibit complex electrical properties akin to that in adult primate fovea
- Stage 3 RO cones are most light-sensitive at the latest time points of maturation

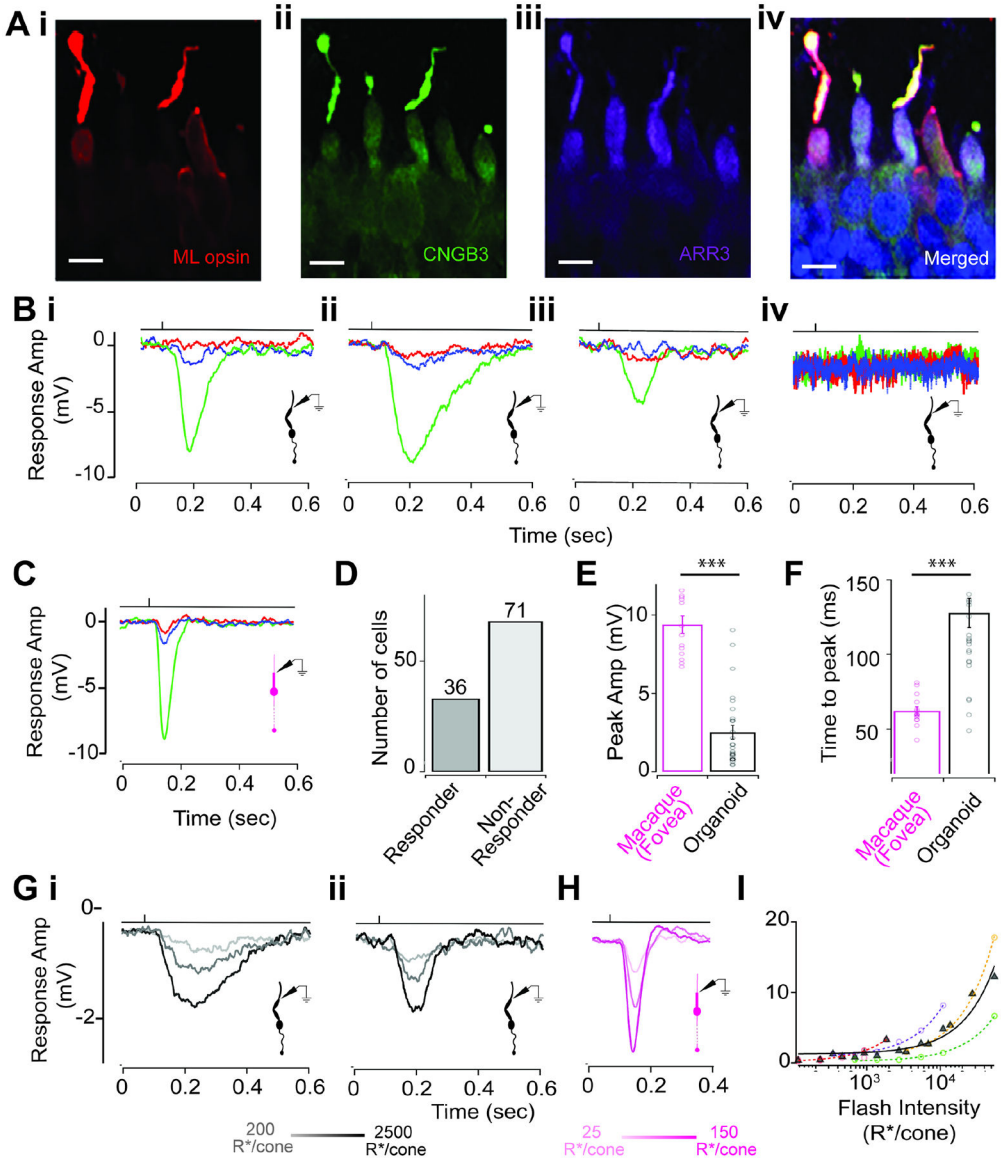

Figure 1: Comparison of light responses from RO cones and primate foveal cones

(A) RO cones labeled for components of the phototransduction machinery. Red, M/L opsin (i); green, CNGB3 (ii); violet, ARR3 (iii); merged (iv). Scale bars: 10 μm.

(B) Exemplar traces showing responses to a 10-ms typing flash stimulus. (i–iv). Henceforth, for all figures, the time point of the light stimulus is denoted by the vertical line above the response traces.

(C) Exemplar response to typing flash stimuli of a macaque foveal cone (M-cone).

(D) Bar plot showing the number of cones that responded to the typing light flash (responders; n = 36) versus those that did not (nonresponders; n = 71).

(E) Comparison of peak amplitude of cone voltage responses to typing flash stimulus in RO cones (black) and macaque foveal cones (magenta) (fovea: 9.37 ± 0.56 mV, n = 14; RO: 2.51 ± 0.45 mV, n = 27; p value = 2.4×10^{-11}).

(F) Voltage responses to the typing flash were slower for RO cones than for macaque foveal cones (foveal cones: 62.2 ± 2.77 ms, n = 14; RO cones: 127.57 ± 9.69 ms, n = 27; p value = 0.00002).

(Gi and Gii) Examples of voltage responses of dark-adapted RO cones to 10-ms flashes of increasing light intensities eliciting 200, 1,000, and 2,500 cone opsin photoisomerizations (R*)/cone/flash.

(H) Exemplar voltage responses of a dark-adapted macaque foveal cone to 10 ms flashes of light intensities of 25, 75, and 150 R*/cone/flash.

(I) RO cone responses did not saturate for flash intensities tested. Response amplitude increased linearly over three orders of magnitude of light flash intensities (black, average response across multiple RO cones; colored traces, response for individual cones). Values in all figures represent mean ± SEM.

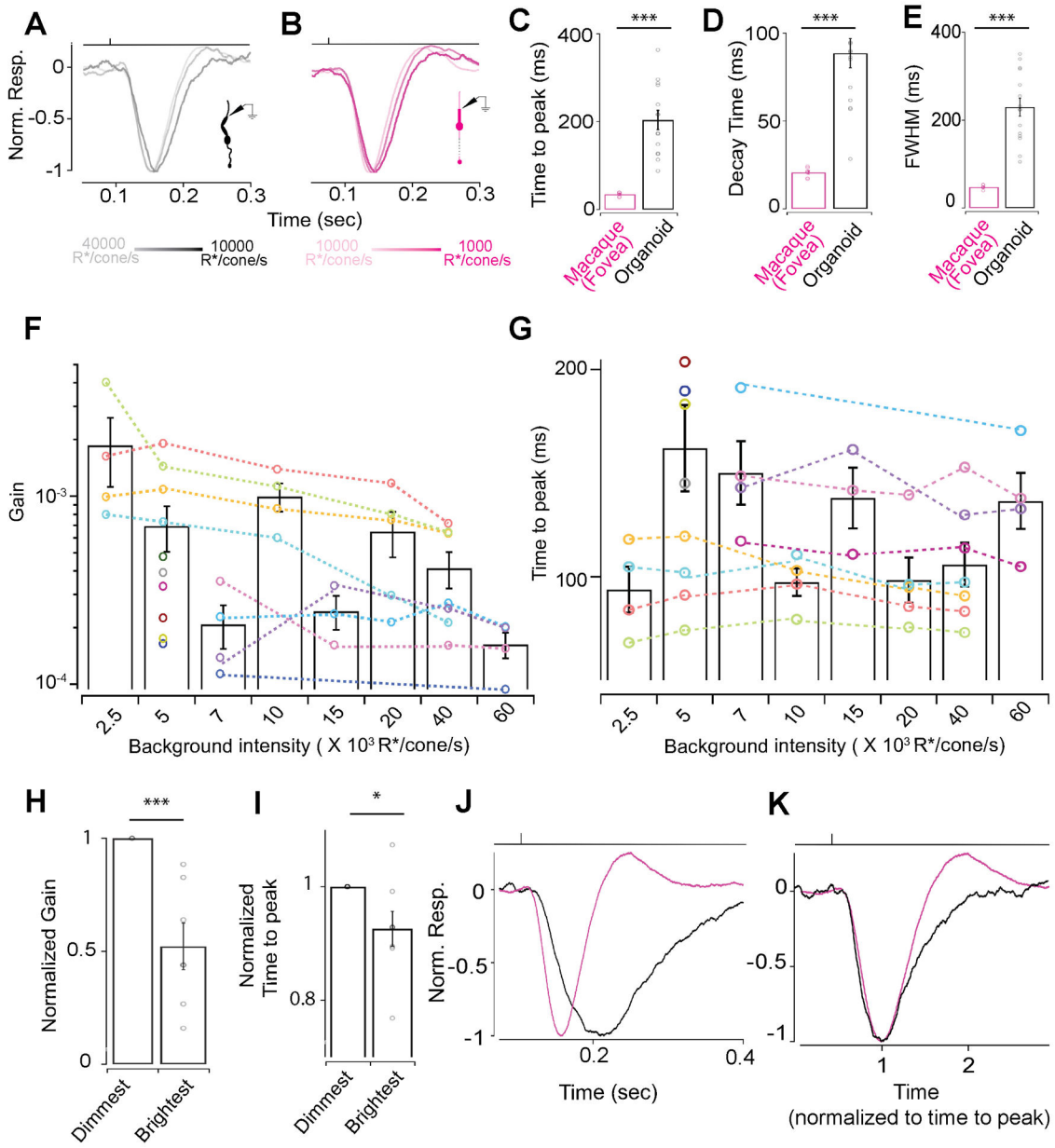

Figure 2: RO cones respond over a wide range of mean luminance.

(A, B) Exemplar voltage responses to 10 ms 200% contrast flashes at varying background luminance. (A) Exemplar voltage responses by a RO cone to a 10 ms 200% contrast flash at 10000, 20000 or 40000 R*/cone/s background light-levels (B). Exemplar voltage responses by a primate foveal cone to a 10 ms 200% contrast flash at 1000, 5000 or 10000 R*/cone/s background light-levels. (C-E) Characterization of the average response of multiple foveal and RO cones to a 10 ms 200% contrast flash at a background of 5000 R*/cone/s. (C) Time to peak for primate foveal cones (34.8 ± 1.73 ms, n=7) and RO cones (203.8 ± 21.1 ms, n=15). Response decay time as in (C) for foveal cones (20.7 ± 1 ms, n=7) and RO cones (88.5 ± 8.4 ms, n=15). (E) Full width at half maxima as in (C) for foveal cones (47.7 ± 1.8 ms, n=7) and RO cones (229.5 ± 20.5 ms, n=15). (F) Gain decreases with

increase in background luminance in individual RO cones (colored lines). Bar graph shows the average gain and the distribution of gain values at a given background luminance across RO cones. (G) Time to peak decreases for individual RO cones over increasing background luminance (colored lines). Bar graph represents the average time to peak and the distribution of times to peak at a given background luminance across RO cones. (H) Gain at the brightest background was normalized by gain at the lowest background luminance for each cell and showed a 50% reduction. (I) Time to peak of the cone light response at the brightest background was normalized by time to peak at the lowest background luminance for each cell and showed a significant increase. (J) Normalized average responses across five RO (black) and foveal (magenta) cones to a 10ms 300% contrast light flash at a background luminance of 5000R*/cone/sec. (K) Average responses shown in panel J superimposed with the time to peak normalized to one.

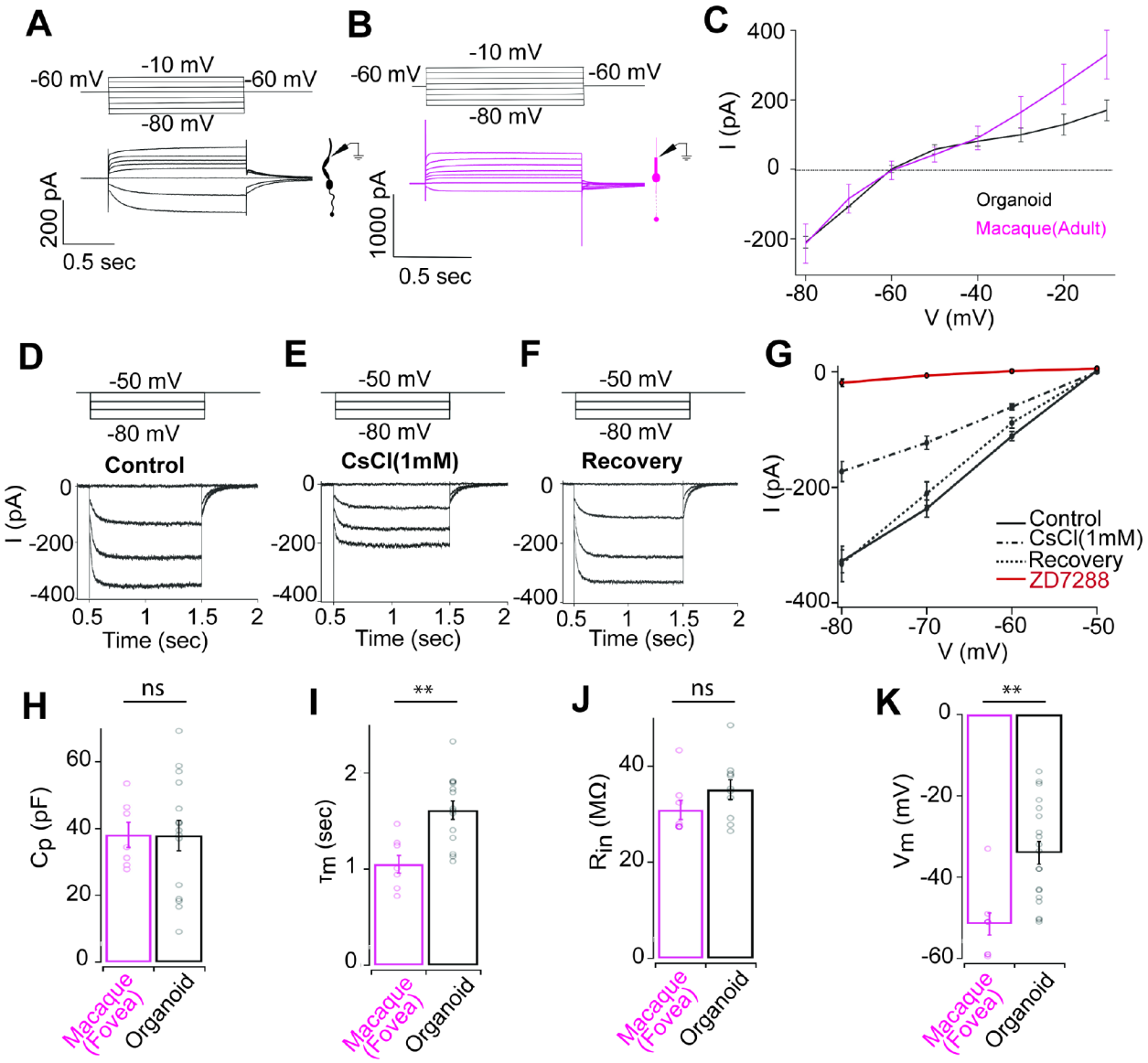

Figure 3: Comparison of passive membrane properties of RO cones and primate foveal cones.

(A, B) Voltage steps (top) and resulting exemplar current responses (bottom) for RO cones (black, A) or macaque foveal cones (magenta, B). (C) Current voltage curve at plateau amplitude for RO cones (black, n=15) or primate foveal cones (magenta, n=9). (D–F) Whole cell voltage clamp recording from an individual RO cone, showing leak-subtracted HCN currents (bottom traces) in response to four hyperpolarization steps (top traces) from a holding potential of −50 mV (10 mV increase per step). (D) response before drug treatment (E) after application of 1 mM CsCl. (F) Response after wash-out of 1 mM CsCl. (G) Current voltage curve at plateau amplitude for (D–F). (H) Average measured membrane capacitance of RO cones (37.9 ± 4.6 pF, n=15) or macaque foveal cones (38.1 ± 3.8 pF, n=7). (I) Average measured membrane time constant for RO cones (1.62 ± 0.1 s, n=14) or primate foveal cones (1.1 ± 0.1 s, n=8). (J) Measured average input resistance for RO cones (35.1 ± 2.1 MΩ, n=10) or primate foveal cones (30.9 ± 2 MΩ, n=8). (K) Average measured resting

membrane potential for RO cones (−34 ± 2.8 mV, n=19) or primate foveal cones (−51.5 ± 2.7 mV, n=9).

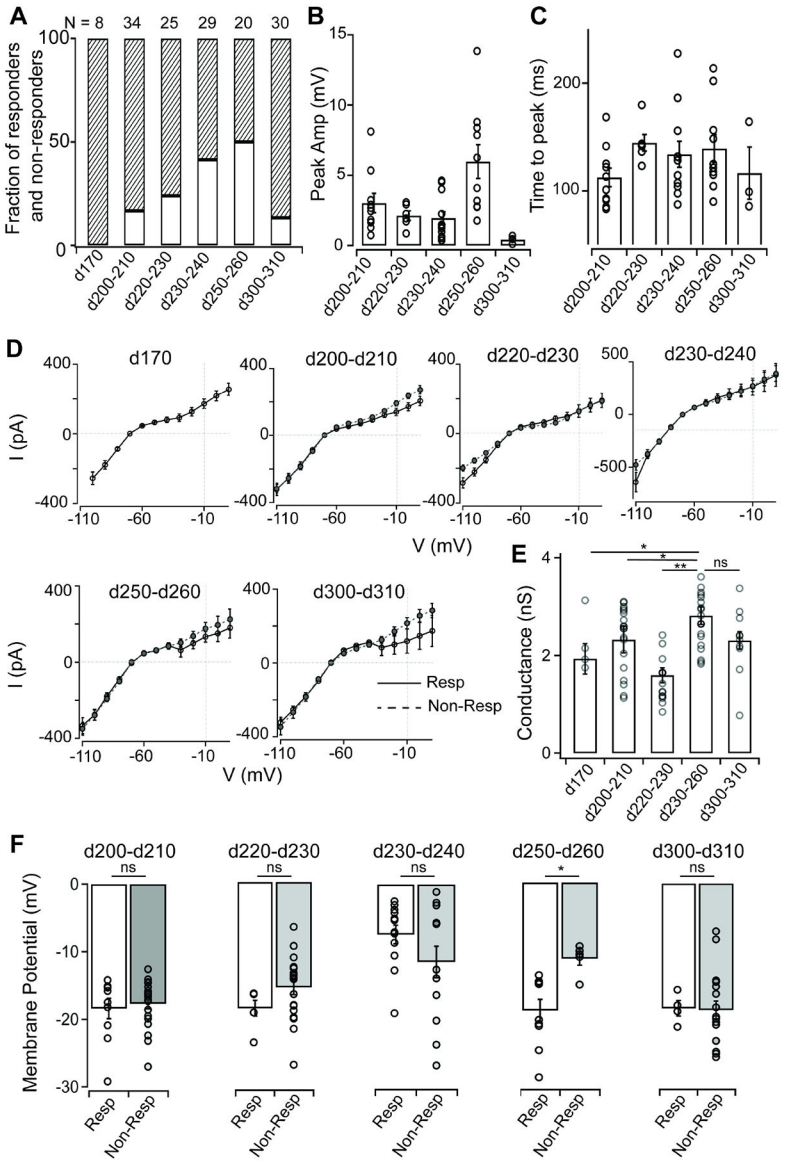

Figure 4: Comparison of light evoked responses and passive membrane properties of RO cones across different developmental timepoints.

(A) Fraction of responders versus nonresponders in stage 3 RO cones from WA09 organoids cultured for increasing amounts of time.

(B) Comparison of peak amplitude of RO cone voltage responses to a brief flash of light (~500,000 R*/cone/s) across time points (d200–d210: 3.02 ± 0.69 mV, n = 10; d220–d230: 2.13 ± 0.33 mV, n = 6; d230–d240: 1.95 ± 0.45 mV, n = 12; d250–d260: 5.97 ± 1.20 mV, n = 10; d300–d310: 0.42 ± 0.17 mV, n = 3). RO cones at d250–d260 had the maximum sensitivity to the light flash.

(C) Time to peak is consistent for RO cone voltage responses to a brief flash of light (~500,000 R*/cone/s) across developmental time points (d200–d210: 112.35 ± 8.69 ms, n = 10; d220–d230: 144.58 ± 7.68 ms, n = 6; d230–d240: 133.79 ± 12.09 ms, n = 12; d250–d260: 139.33 ± 12.96 ms, n = 10; d300–d310: 116.30 ± 24.21 ms, n = 3).

(D) Comparison of current-voltage (I–V) curves for responder and nonresponder RO cones at different developmental time points. RO cones at later stages of development (>d230) had greater hyperpolarization-activated currents.

(E) RO cones at d230–d260 of development had maximal ion conductance at hyperpolarizing membrane potentials (−100 mV, liquid junction potential corrected) (d170: 2.83 ± 0.39 nS, n = 4; d200–d210: 2.89 ± 0.05 nS, n = 19; d220–d230: 2.04 ± 0.18 nS, n = 15; d230–d260: 2.81 ± 0.18 nS, n = 20; d300–d310: 2.90 ± 0.25 nS, n = 10) (d170 vs d230–260, p value = 0.015; d200–210 vs d230–260, p value = 0.045; d220–230 vs d230–260, p value = 0.007; d300–310 vs d230–260, p value = 0.079).

(F) Resting membrane potential of responder versus nonresponder RO cones at different time points of development. Apart from d250–d260 time point of development, there was no significant difference between responders and nonresponders at any other time points. Responder RO cones at d230–d240 were also significantly depolarized compared with their counterparts at other time points (d200–210, p value = 0.69; d220–230, p value = 0.07; d230–240, p value = 0.15; d250–260, p value = 0.0015; d300–310, p value = 0.89).

Key resources table:

REAGENT or RESOURCE	SOURCE	IDENTIFIER
Antibodies		
ARR3	Novus	RRID:AB_2060085
CNGB3	Santa Cruz	RRID: AB_2895311
ML Opsin	Millipore	RRID: AB_177456
NR2E3	Abcam	RRID: AB_776860
Normal Donkey Serum	Millipore	S30-100
Bovine Serum Albumin	Sigma-Aldrich	A7906-100G
Triton	Sigma-Aldrich	X100-100
Anti-Mouse Alexa Fluor 488	ThermoFisher Scientific	A21202
Anti-Rabbit Alexa Fluor 546	ThermoFisher Scientific	2128963
Anti-Goat Alexa Fluor 633	ThermoFisher Scientific	A21082
Prolong Gold antifade + DAPI	ThermoFisher Scientific	P36931
Biological samples		
Macaque retina	Wisconsin National Primate Center	
Chemicals, peptides, and recombinant proteins		
Ames	Sigma	1420
Deoxyribonuclease A	Sigma	D4527
ZD7288 hydrate	Sigma Aldrich	Z3777
CsCl	Sigma Aldrich	C4036
Glutaraldehyde 8%	Electron Microscopy Sciences	16019
Paraformaldehyde	Electron Microscopy Sciences	15710
Sodium Cacodylate	Electron Microscopy Sciences	11650
rhBMP-4	R&D Systems	314-BP
Chemically Defined Lipid Supplement	ThermoFisher Scientific	11905031
Poly(2-hydroxyethyl methacrylate): PolyHEMA	Sigma-Aldrich	P3932-25G
ReLeSR	Stem Cell Technologies	05872
ROCK inhibitor Y-27632	R&D Systems	1254
Pioloform powder	Ted Pella Inc.	19244
Experimental models: Cell lines		
WA09	WiCell	RRID:CVCL_9773
1581	Capowski et al. 2019	RRID:CVCL_B3UV
1013	Capowski et al. 2019	RRID:CVCL_B3UR
2429		RRID:CVCL_2769
Software and algorithms		
IGOR Pro	WaveMetrics	https://www.wavemetrics.com/

REAGENT or RESOURCE	SOURCE	IDENTIFIER
MATLAB	Mathworks	https://ch.mathworks.com/products/matlab
Symphony	Symphony-DAS	https://github.com/symphony-das
ImageJ	NIH	https://imagej.nih.gov/ij/
Other		
Superfrost Plus Slides	Electron Microscopy Sciences	12-550-15